Electronic Supplementary Material (ESI) for Journal of Materials Chemistry A.

Evolution of Ni/Li Antisites under the Phase Transition of Layered $LiNi_{1/3}Co_{1/3}Mn_{1/3}O_2$ Cathode

Ang Gao[1,2], Yang Sun[1], Qinghua Zhang[2], Jieyun Zheng[2] and Xia Lu[1,*]

1 School of Materials, Sun Yat-sen University, Guangzhou 510275, China

2 Beijing National Laboratory for Condensed Matter Physics, Institute of Physics, Chinese Academy of Sciences, Beijing 100190, China

E-mail: luxia3@mail.sysu.edu.cn (X. Lu)

Description of Supplementary Files

File name: Supplementary Information

Description: Supplementary figures, supplementary tables, and supplementary references.

File name: Supplementary Movie

Description: Animation of Ni and Li ion diffusion trajectories for Ni/Li antisites formation.

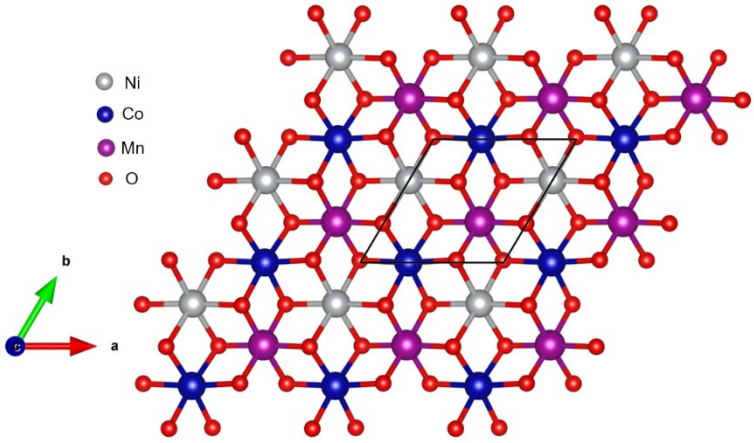

Figure S1. Long-range order (LRO) distribution of TM ions in the TM layer of NCM111, remaining 1:1:1 of the Ni:Co:Mn ratio in each TM layer.

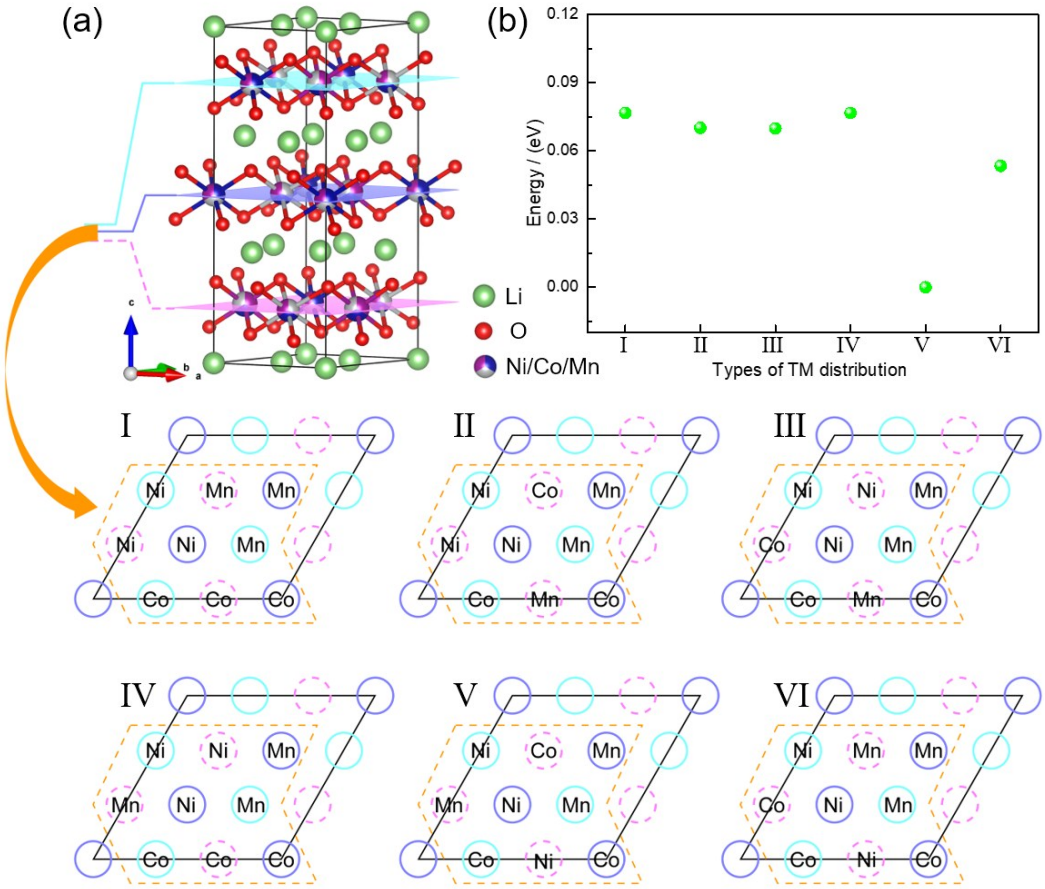

Figure S2. Optimizing stackings of TM layer along the ***c***-axis in layered NCM111. (a) the NCM111 supercell with $[\sqrt{3}a\times\sqrt{3}b\times 1\boldsymbol{c}]$R30°, corresponding to six stacking modes of TM layer. Cyan, blue and pink circles represent TM ions in the first, second and third TM layer, respectively. Solid circles mean the fixed distribution of ions, and dotted circles mean the variable distribution of ions. (b) Formation energies of layered NCM111 with different stacking modes of TM layer obtained using DFT-based first principles calculations.

Note that The layered NCM111 is belong to O3-type structure, that is the stacking period of transition metal layer is three. First, we choose any layer as the stacking standard, here is the second TM layer (blue solid circles). Then, the distribution of the first layer relative to the second layer was considered, which is only one configuration. So the first TM layer also is fixed as shown in cyan solid circles. Finally, the distributions of the third layer (pink dotted

circles) relative to the other two layers is six kinds, implying six stacking modes of TM layer. Local environments are similar among different stacking modes. The manner to stack layers seems to have little influence on the crystal and electronic structures due to the equivalency of Co, Ni, and Mn positions in the superlattice. Hence the difference between different stacking methods is often overlooked. Here, detailed stacking modes were enumerated and optimized, among which the maximum energy difference is 77 meV, corresponding to 8.6 meV per formula unit ($LiNi_{1/3}Co_{1/3}Mn_{1/3}O_2$). The interaction between adjacent layers mainly is van der waals force. Although previously not considered as a genuine or primary type of chemical bonding, the intermolecular forces arising from induced instantaneous polarization multipoles in molecules (van der Waals forces) can become quite attractive when the interacting species are large.[1] In addition, the stacking manner maybe influence the the superexchange interaction and the magnetic frustration to modulate the total energy.[2, 3] The reason why is type V configuration more favorable remain unclear, which is the most stable configuration according to the energy.

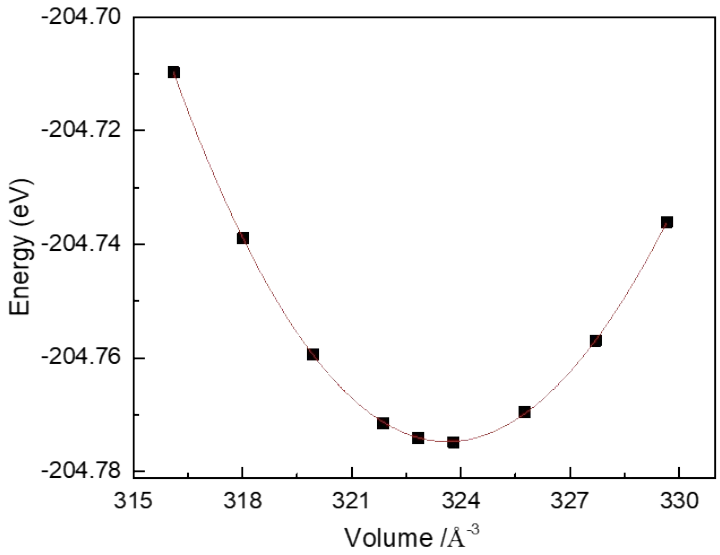

Figure S3. The plot that the energy-volume data were fitted to a third-order Birch-Murnaghan equation of state (EOS) and the parameters were shown in Table S3.

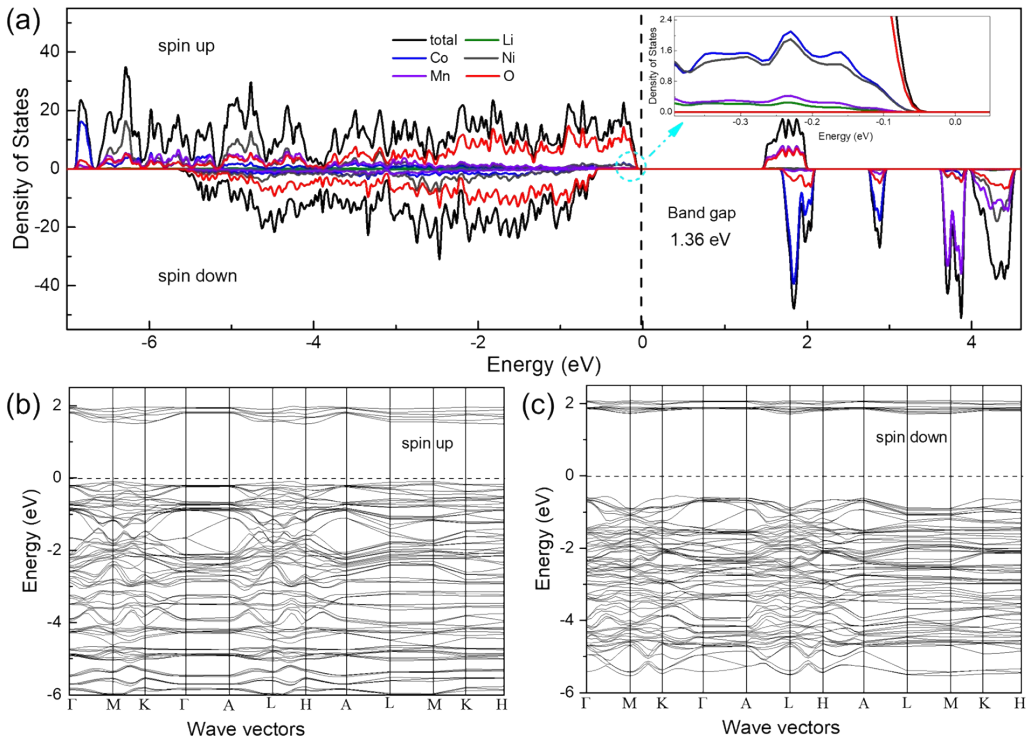

Figure S4. Electronic structure of $LiNMC_{1/3}O_2$ with $[\sqrt{3}a\times\sqrt{3}b\times 1\boldsymbol{c}]$R30° supercell. (a) Density of states (DOS). The zero energy is set to the Fermi level. Positive and negative states represent spin up and spin down states, respectively. (b) band structure (spin up). (c) band structure (spin down). The coordinates of high symmetry K-points are Γ (0 0 0), M (1/2 0 0), K (1/3 1/3 0), A (0 0 1/2), L (1/2 0 1/2) and H (1/3 1/3 1/2) in hexagonal lattice.

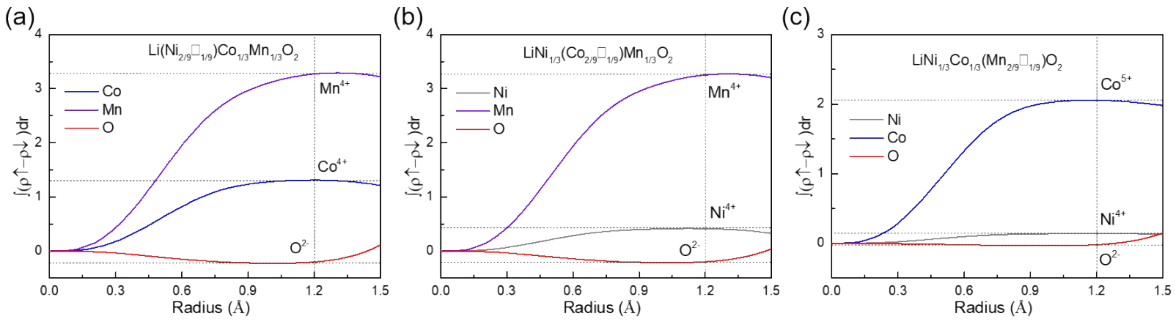

Figure S5. Integrated spin as a function of the radius around Ni, Co, Mn and O ions in layered $LiNMC_{1/3}O_2$ with (a) Ni vacancy defect, (b) Co vacancy defect and (c) Mn vacancy defect.

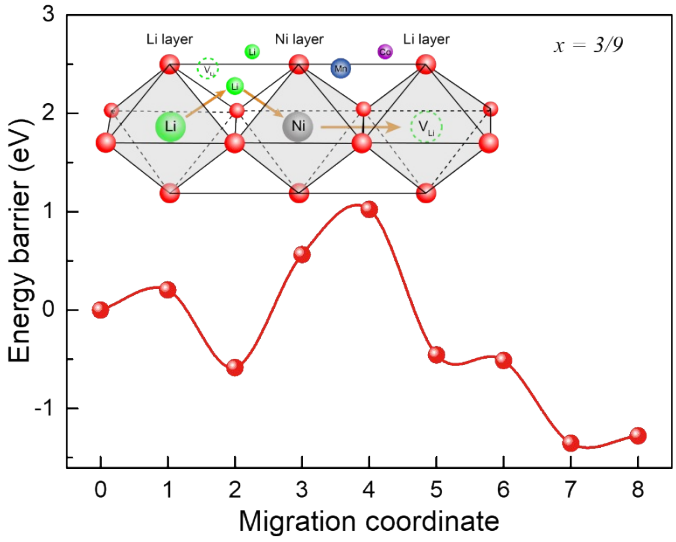

Figure S6. Migration energy barriers calculated with the CI-NEB method for linear exchange trajectory containing divacancy mechanism of Li ion illustrated in the inset in $Li_{1-x}NCM_{1/3}O_2$ ($[\sqrt{3}a\times\sqrt{3}b\times1\boldsymbol{c}]$R30°) at the SOC of x = 3/9.

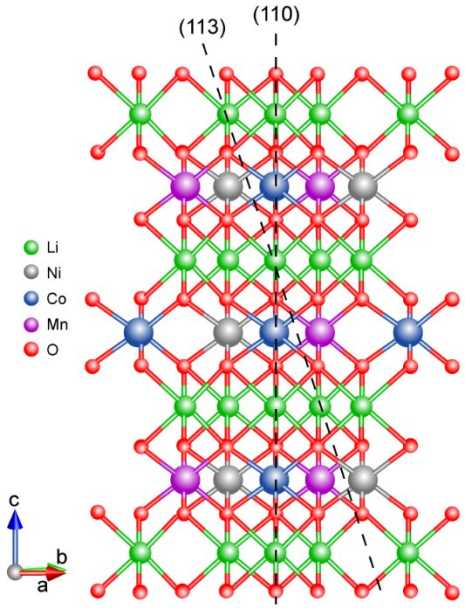

Figure S7. The illustration of planes in O3-type NCM111, including (110) and (113), which is associated with Figure 5.

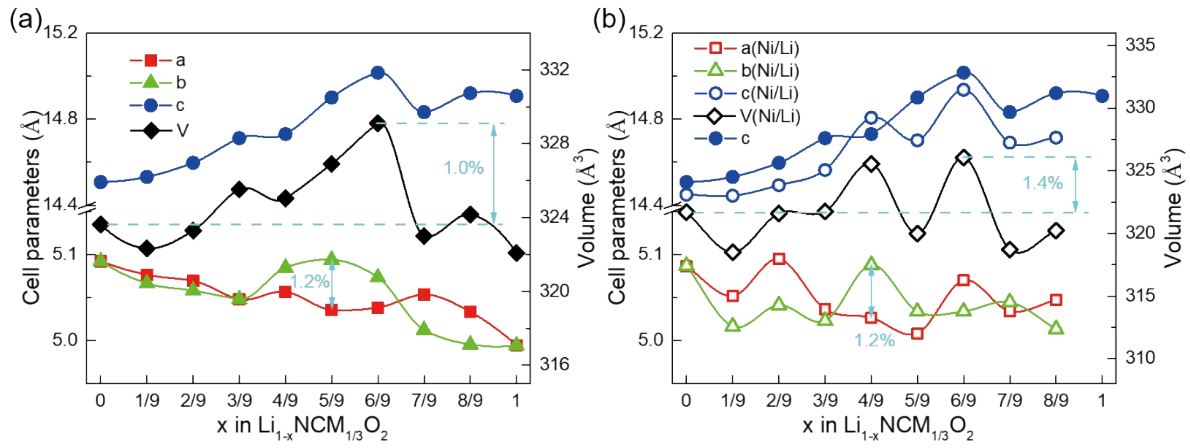

Figure S8. (a) The lattice parameters and volume of $Li_{1-x}NCM_{1/3}O_2$ ($[\sqrt{3}a\times\sqrt{3}b\times 1\boldsymbol{c}]R30°$) without Ni/Li antisites at different SOC (x = 0 ~ 1). (b) The lattice parameters and volume of $Li_{1-x}NCM_{1/3}O_2$ with Ni/Li antisites at different SOC (x = 0 ~ 1) and the $\boldsymbol{c}$ of $Li_{1-x}NCM_{1/3}O_2$ without Ni/Li antisites also is drawn to compare.

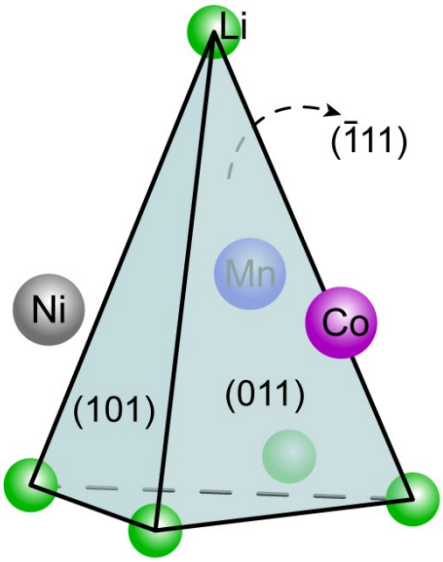

Figure S9. The illustration of planes based on unit cell with 1×1×1 belongs to family of crystal planes {101} but with different direction in O3-type NCM111.

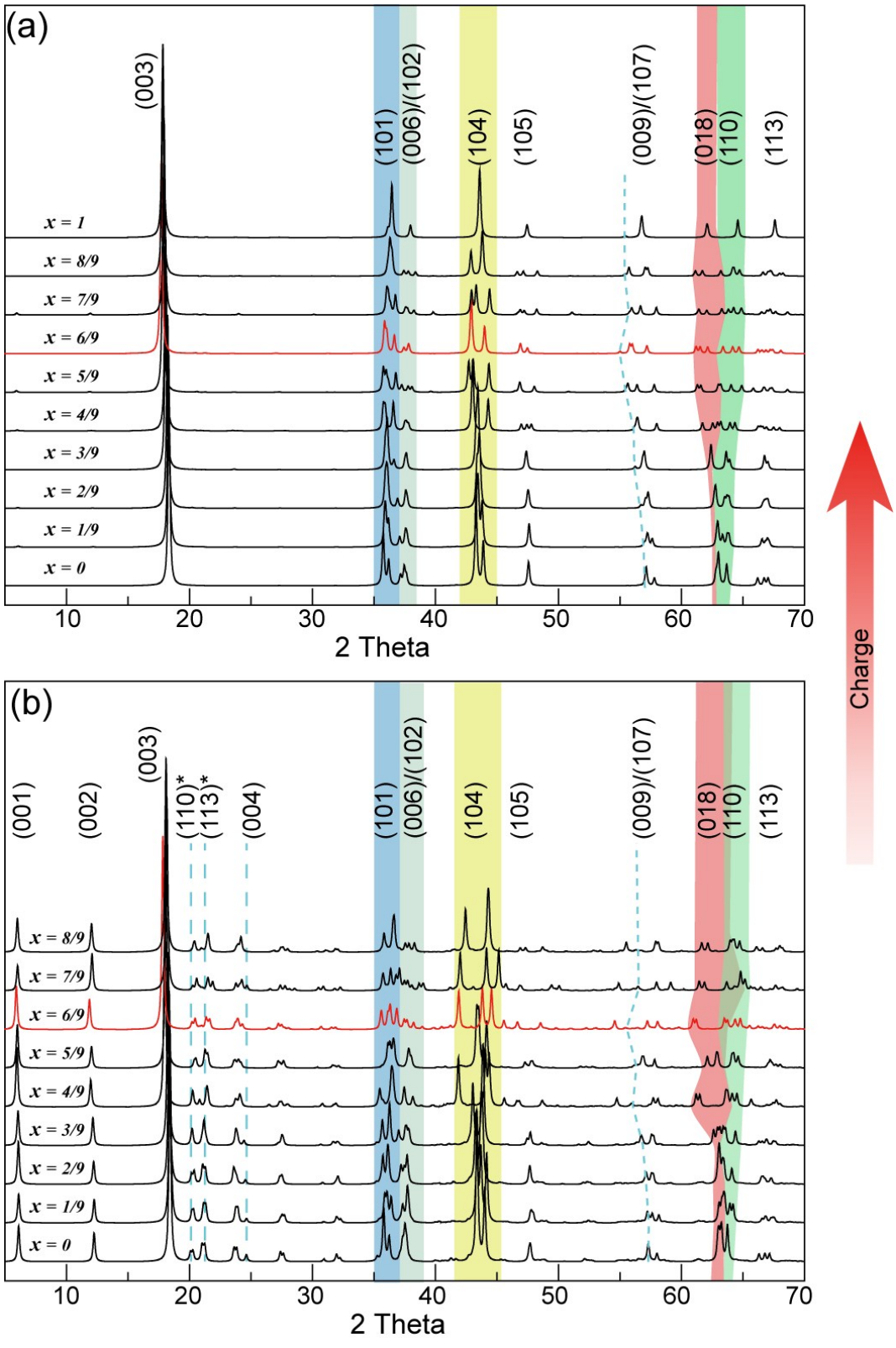

Figure S10. Simulative XRD patterns of $Li_{1-x}NCM_{1/3}O_2$ (a) without and (b) with Ni/Li antisites.

Table S1. The atomic chemical potentials (μ_i) by DFT-based calculations in bulk metals (Li and TM) or vacuum layer (O_2) at 0 K with different space groups.

Atom type	Space Group	Total energy/eV	Atom number	Energy per atom/eV
Li	$FM\bar{3}M$	-7.64	4	-1.910
	$I\bar{4}3D$	-30.42	16	-1.901
	$IM\bar{3}M$	-3.80	2	-1.899
	$P6_3MMC$	-3.77	2	-1.886
	$P4_132$	-6.55	4	-1.638
	$R\bar{3}MH$	-5.62	3	-1.874
Ni	$FM\bar{3}M$	-6.63	4	-1.657
	$P6_3MMC$	-3.19	2	-1.593
Co	$FM\bar{3}M$	-14.23	4	-3.557
	$P4_2MNM$	-98.27	28	-3.510
	$P6_3MMC$	-6.26	2	-3.132
Mn	$FM\bar{3}M$	-24.82	4	-6.206
	$I\bar{4}3M$	-286.68	58	-4.943
	$P4_132$	-123.49	20	-6.175
O	-	-3.56	2	-1.780

Table S2. The comparisons between the fitted parameters and the experimental data for NCM111 ($R\bar{3}m$) from neutron diffraction Rietveld.

Source	Unit cell	E_0/eV	V_0/Å^3	B_0/GPa	B_1	a/Å	b/Å	c/Å	α/°	β/°	γ/°
Cal. (this work)	$[\sqrt{3}a\times\sqrt{3}b\times 1\boldsymbol{c}]$R30°	-204.8	323.6	113.9	4.66	5.092	5.092	14.508	90.25	89.75	59.35
	1×1×1	-	107.9	-	-	2.940	2.940	14.508	-	-	-
Exp.[4]	1×1×1	-	100.8	-	-	2.860	2.860	14.227	-	-	-

E_0 denotes the intrinsic energy at zero pressure.

V_0 is the volume at zero pressure.

B_0 is the bulk modulus.

B_1 is the first pressure derivative of the bulk modulus.

a, b, c, α, β, γ are the cell parameters.

Table S3. Contrast of Miller indices based on cells with 1×1×1 and $[\sqrt{3}a\times\sqrt{3}b\times 1\boldsymbol{c}]$R30°.

1×1×1[a]	$[\sqrt{3}a\times\sqrt{3}b\times 1\boldsymbol{c}]$R30° [b]
(003)	(003)
(101)	(211), ($\bar{1}\bar{2}$1), ($\bar{1}$11)
(006)	(006)
(102)	(122), ($\bar{2}\bar{1}$2), (1$\bar{1}$2)
(104)	(214), ($\bar{1}\bar{2}$4), ($\bar{1}$14)
(105)	(125), (1$\bar{1}$5), ($\bar{2}\bar{1}$5)
(009)	(009)
(107)	(217), ($\bar{1}\bar{2}$7), ($\bar{1}$17)
(018)	(128), ($\bar{2}\bar{1}$8), (1$\bar{1}$8)
(110)	(330)
(113)	(333), (303), (033)

[a] only the customary plane indices among family of crystal planes based on unit cell with 1×1×1 were listed.

[b] The plane indices involving three directions based on unit cell with $[\sqrt{3}a\times\sqrt{3}b\times 1\boldsymbol{c}]$R30° were listed.

Supplementary References

1 L. Zhao, M. Hermann, W. H. E. Schwarz and G. Frenking, *Nature Reviews Chemistry*, 2019, **3**, 48-63.

2 J. Zheng, G. Teng, C. Xin, Z. Zhuo, J. Liu, Q. Li, Z. Hu, M. Xu, S. Yan, W. Yang and F. Pan, *J. Phys. Chem. Lett.*, 2017, **8**, 5537-5542.

3 Y. Xiao, T. Liu, J. Liu, L. He, J. Chen, J. Zhang, P. Luo, H. Lu, R. Wang, W. Zhu, Z. Hu, G. Teng, C. Xin, J. Zheng, T. Liang, F. Wang, Y. Chen, Q. Huang, F. Pan and H. Chen, *Nano Energy*, 2018, **49**, 77-85.

4 S.-C. Yin, Y.-H. Rho, I. Swainson and L. F. Nazar, *Chem. Mater.*, 2006, **18**, 1901-1910.